ELSEVIER

Biochimica et Biophysica Acta 1281 (1996) 189–204

BBA Biochimica et Biophysica Acta

Assessment of molecular sieving across bacterial outer membrane of *Pseudomonas*

Satish B. Kulkarni, V. Somlata, V. Sitaramam *

Department of Biotechnology, University of Pune, 411 007 Pune, India

Received 22 November 1995; revised 15 January 1996; accepted 15 January 1996

Abstract

The role of the permeability barrier of the outer membrane of *Pseudomonas* was re-evaluated based on the physical theory of molecular sieving in view of its intrinsic antibiotic resistance. We developed a set of analytical procedures based on parametric and non-parametric statistical tests to evaluate, validate and adopt the better among a set of competing non-linear models of diffusion. The molecular mass dependence of uptake of non-electrolytes in bacteria yielded a quantitative measure to distinguish between sieving mechanisms and specific uptake/efflux mechanisms. The experimental data, supported by the physical model of DEAE-Sephadex and various analytical models and extensive simulation of the errors, both in measurement and models, yielded evidence consistent with the relaxation of the outer membrane matrix barrier in *Pseudomonas*.

Keywords: Renkin's equation; Pore size; Error simulation; Outer membrane; Nonelectrolyte; Diffusion; (*P. aeruginosa*)

1. Introduction

Exposure of bacteria to antibiotics is limited by the barriers that exist in the cell wall [1], outer membrane [2,3] and the plasma membrane [4,5]. The cytosolic concentration of an antibiotic should relate to the net diffusivity of the antibiotic to the interior. Passive diffusion would necessarily involve molecular sieving of some kind at the level of the outer membrane or cell wall and the plasma membrane. Specific uptake mechanisms enhance the bacterial cytosolic concentrations of the antibiotic [4] while specific degradative and extrusion mechanisms would be expected to lower the antibiotic concentrations in the cytosol [4,5]. The reference base for defining the accessibility of antibiotic to the bacterium therefore must consider the diffusivity based on molecular sieving as a first approximation to decide which mechanism contributes to the levels of antibiotic achieved to account for the cellular pharmacodynamics (Fig. 1). In other words, a rigorous evaluation of the porosity of the outer membrane, cell wall and plasma membrane would considerably aid in a quantitative delineation of the antibiotic handling mechanisms by the bacterium.

While this problem is fairly well understood [1–21] it is by no means resolved [14,15,17–19]. Considerable controversy exists for the relative contribution of various mechanisms in specific bacteria such as *Pseudomonas aerugi-*

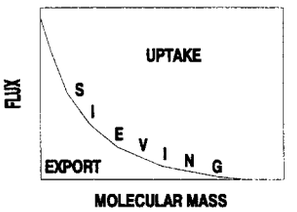

Fig. 1. Theoretical model illustrating the sieving, uptake and export mechanism of solutes in the membrane. Solutes visualized are either non-electrolytes or non-ionized molecules. Theoretical plot of flux vs. molecular mass of solutes is predicted from the Renkin's equation (see text). If a flux of a particular molecule deviates from the predicted profile then it reflects the presence of either a uptake or export mechanism for that molecule. Typically a large molecular mass species showing a higher flux indicates the existence of an uptake mechanism. Similarly a lower molecular mass species with low flux suggests the possibility of an export mechanism.

* Corresponding author. Fax: +91 212 355179.

PII S0005-2736(96)00010-7

nosa [8,14–19], not because of faulty experiments but apparently because of a lack of consensus on what is the best experimental strategy and the best way to analyze the data. The antibiotic resistance of *Pseudomonas aeruginosa* is important because infections by this organism, systemic and topical, opportunistic or otherwise, are of increasing importance in clinical and veterinary medicine [4,6,7]. The general resistance of this organism has been attributed to low permeability of the outer membrane [2,7–13]. The permeability of this membrane to β-lactam antibiotics and some other agents was shown to be 2–3 orders of magnitude lower than for *Escherichia coli* [2,13]. It was claimed that the exclusion limit of outer membrane of *Pseudomonas* is less than the size of a disaccharide [14,15], which was considered important in precluding the uptake of most antibiotics [8,15,16]. Controversy persists regarding the exclusion limit (or pore size) and its interpretation [17–19]. The porins could be found even in the cell wall of *Mycobacteria* [1], which are Gram-positive. Thus, a better understanding of the porin pathway would help in design of effective strategies even for antimycobacterial therapy [1]. Therefore an understanding of the barrier (permeability) function of outer membrane and cell wall, in Gram-negative and Gram-positive bacteria, respectively, has immediate implications in combating the antibiotic resistance based on the physiology of these microorganisms.

It appears from claims in the literature that *Pseudomonas* has some unique properties: (i) high and broad drug resistance; (ii) low outer membrane permeability [2,7–13]; (iii) presence of large pore size porins in the outer membrane [17–19]. The latter two pose some difficulties in understanding the intrinsic drug resistance of this organism. Firstly, the reports on the presence of the porin of a large pore size [17–19] in the outer membrane contradicts the finding that the exclusion limit is less than a size of disaccharide [14,15]. Secondly the 'low' outer membrane permeability is actually a self contradiction in literature with attempts to explain the coexistence of large pores in the membrane [18]. These issues are further and even more complicated by the use of different analytical methods for the estimation of pore size [14–20].

We re-examined the published and our own results in this regard to arrive at a standardized analytical procedure for evaluation of the porosity of the bacterial outer membrane. The data and the statistical analyses show that while arguments abound regarding the permeability limits of the outer membrane [14–19], in actual fact the world literature is fairly converging to a value of approx. 8–9 Å for the porin in the *Pseudomonas* species. We highlight the utility of the procedure to determine the porosity of the outer membrane matrix of *Pseudomonas* species as well as its applicability to the question of modifications in the permeability by adjuvants. The experimental data is fairly conclusive that the outer membrane matrix, presumably involving porins, can be dilated by the addition of ionic detergents.

2. Materials and methods

2.1. Materials

2.1.1. Bacterial strains

Pseudomonas aeruginosa NCIB 8650 (National Collection of Industrial Bacteria, Torry Research Station Aberdeen, UK) was obtained from National Collection of Industrial Microorganisms, Pune (India); another strain of *Pseudomonas aeruginosa* was isolated from soil. *Escherichia coli* K12 (wild type) and *Staphylococcus aureus* (a clinical isolate) were also used. *Pseudomonas aeruginosa* strain NCIB 8650 was specifically chosen for its non-pigment characteristic. This made the absorbance measurements easier for PCV and turbidity analysis (see below).

2.1.2. Media

Bacterial cultures were grown in Luria broth or in minimal medium at 37°C using a rotary shaker. Luria broth contained 1% tryptone, 0.5% yeast extract and 0.5% NaCl. The composition of minimal medium was; 1 mM KH_2PO_4, 1.5 mM $(NH_4)_2SO_4$, 0.08 mM $MgCl_2$, 1.8 μM $FeSO_4$, 40 mM sodium-phosphate buffer (pH 7.2) and 0.2% glucose.

2.1.3. Chemicals

The detergents, DEAE-Sephadex (A-25–120) and non-electrolytes were obtained from Sigma (USA). Blue dextran 2000 was from Pharmacia (Sweden). All other reagents were of analytical grade.

2.2. Methods

2.2.1. Measurement of permeability to non-electrolytes

A molecule that cannot cross the outer membrane would be a marker for the extracellular space by which one can measure the packed cell volume of an aliquot of bacteria. When this aliquot is placed in a hypertonic medium of a non-electrolyte, the cells shrink and plasmolysis ensues [14,15]. The difficulty is in distinguishing between the classic case of selective plasma membrane shrinking as opposed to both the cell wall and the plasma membrane collapsing. If the external osmolyte penetrates the outer membrane, the cell expands enhancing the packed cell volume as sensed by the high molecular weight impermeant marker. The method is also quantitative in so far as the reflection coefficient to the non-electrolyte is concerned. Packed cell volume (PCV) was measured from the blue dextran inaccessible space. Blue dextran was used as a marker for extracellular space; cells did not take up any blue dextran during the incubation period nor was any found bound to the membrane. This was checked by doing detailed recovery experiments after centrifugation as a function of bacterial concentration as well as blue dextran concentration. The PCV values obtained were independent of blue dextran concentration, which indicated the absence

of any measurable binding interaction. Lastly the PCV varied nearly linearly with the density of bacteria used (data not given). Electron microscopy in cells fixed by glutaraldehyde was often claimed to be useful to distinguish between the cell wall collapse and plasma membrane collapse [14,21]. However, our experience with erythrocyte stability, particularly due to removal of fixed amino-group charges by cross-linking with consequent drastic changes in permeability in red cells (unpublished observations) has precluded us from assigning any reliability to electron microscopic studies in this regard.

Bacteria were grown in Luria broth containing 5 mM $MgCl_2$ at 37°C and harvested in mid-log phase, and resuspended in the buffer A (25 mM sodium phosphate, pH 7.4 and 5 mM $MgCl_2$) containing 0.14 M NaCl (total osmolality $\approx$ 325 mosmol/kg). This suspending medium was chosen because it was nearly isotonic for the bacteria [22] and the presence of Mg^{2+} ensured the possible divalent interactions required for the integrity of the outer membrane. All the test solutes were dissolved in buffer A and their osmolality was adjusted to 980 mosmol/kg. The solute entry was measured as an increase in PCV from the hypertonicity to obtain good signal to noise ratios. Blue dextran (5 mg/ml) was dissolved along with test solute; 20 μl of buffer A was added in the case of control cells to 200 μl of this dye solution and 20 μl of appropriate concentration of stock SDS in the case of SDS-treated cells. Finally, 100 μl of stock bacterial suspension was added such that cells were exposed to a corrected osmolality of $\approx$ 792 mosmol/kg for each test solute, i.e., a hypertonic medium. The suspension was incubated for 15 min at room temperature (22°C) and then centrifuged at 10000 $\times g$ for 15 min and the supernatant (200 μl) aspirated and diluted 5-times in buffer A prior to the absorbance measurement. Absorbance of the blue dextran was measured at two wavelengths, 618 and 790 nm the former being the absorbance maximum and latter being a non-absorbing wavelength for blue dextran. The differential absorbance (OD_{618}–OD_{790}) was calculated. In addition, absorbance was measured in cell-free supernatants at similar wavelengths to ensure the complete pelleting of bacteria. Bacteria were added to a solution of the test solute (i.e., without blue dextran) and, after incubation and centrifugation, the absorbance was measured in the supernatant. This served as a blank for the supernatants obtained in the presence of bacteria, which was subtracted from that obtained together with blue dextran. Contribution to the blank by bacteria per se was very little as compared to the blue dextran absorbance, since the latter was measured as the difference in absorbance at two wavelengths. The actual dilution of blue dextran in the absence of bacteria was simultaneously measured by taking 200 μl of test solute, 20 μl of buffer A and 100 μl of buffer A containing 0.14 M NaCl. The OD measurements were by signal averaging of 30 spectra using a computerized (HP 8450A) diode array spectrophotometer.

In all the experiments ($n = 4$), the PCV of the stock bacterial suspension was measured (48% $\pm$ 3) after harvesting the culture in buffer A containing 0.14 M NaCl. The assay was done in triplicate and the percent PCV was calculated from the corrected blue dextran OD obtained in the presence (B) and in the absence (A) of bacteria and multiplying these by corresponding dilution factors, i.e.,

$$\%\ \mathrm{PCV} = \frac{(320 - [(A \times 8 \times 200)/(B \times 5)]) \times 100}{320} \quad (1)$$

The non-electrolytes used were urea, ethylene glycol, propylene glycol, thiourea, glycerol, diethyl urea, erythritol, 2-deoxyribose, fructose, mannitol, sucrose and raffinose, which were successfully employed for similar measurements in a variety of experimental situations by Goldstein and Solomon [23], Lieb and Stein [24], etc.

2.2.2. Measurement of permeability by turbidity changes

Bacterial cultures were grown at 37°C and harvested in mid-log phase of growth. *E. coli* was grown in the minimal medium and *Pseudomonas* in Luria broth. Bacterial cells were washed thrice by centrifuging the cells at 10000 $\times g$ at 4°C. *E. coli* cells were washed in 100 mM sodium-phosphate buffer (pH 7.4) and *Pseudomonas* cells in buffer A containing 0.14 M NaCl. To monitor turbidity changes cells were acutely suspended in different non-electrolyte medium containing 10 mM sodium phosphate (pH 7.4) with and without detergent at 37°C. The osmolality of the non-electrolyte medium was adjusted to 300 mosmol/kg, since it is nearly isotonic [22]. Absorbance changes at 420 nm, a convenient and sensitive non-absorbing wavelength were recorded for upto 3 min under constant stirring using Hewlett Packard diode array spectrophotometer (HP 8450A) and initial rates were calculated. Linearity of response in change in turbidity with the amount of bacteria added was routinely determined. Specific activity was expressed as ΔOD/min per mg of total bacterial protein. The non-electrolytes used were urea, glycerol, erythritol, glucose, galactose, mannitol, lactose, sucrose, trehalose, melezitose, raffinose.

2.2.3. Measurement of K_{av} for different solutes on DEAE-Sephadex column

DEAE-Sephadex columns (0.9 cm i.d. and 30 cm height) were packed after equilibration with distilled water or 1 M NaCl at room temperature. Different solutes were independently eluted and K_{av} values were calculated,

$$K_{av} = (V_e - V_o)/(V_t - V_o), \quad (2)$$

where V_e is the elution volume of the specific solute, V_o, the void volume and V_t is the total exchangeable water space, which was conveniently measured using hydrogen peroxide. Solutes used were, glycerol, mannitol, sucrose, raffinose, stacchyose. Void volume calculations were car-

ried out using Dextran T-70. Fractions were assayed for the solutes by different procedures as described earlier [25].

2.2.4. Polarographic measurement of respiration

Bacterial cells were harvested in mid-log and washed thrice in buffer A containing 0.14 M NaCl at 10 000 × *g* at 4°C. Rate of respiration due to endogenous substrates was measured polarographically with a Clark type oxygen electrode (Gilson) at 37°C. Respiratory rates obtained were expressed as nanoatoms of oxygen consumed per min per mg of protein. Protein was estimated by the method of Lowry et al. [26]. The non-electrolytes used for respiration measurements were urea, ethylene glycol, thiourea, diethyl urea, erythritol, fructose, mannitol, sucrose, trehalose, raffinose.

3. Results

3.1. Theoretical considerations

Presence of a pore in the membrane would affect the observed osmotic pressure for a given solute. A solute would be less of an osmolyte to the extent that it is permeable to the membrane. Strictly speaking one should directly measure the flux rates of various solutes and that of water and determine reflection coefficient of the membrane to a variety of solutes [27]. This macro-description would correspond to an equivalent pore radius which adequately explains the observed non-linearity between the solute flux and the molecular masses of the solutes. This solution phase technique measures the permeability in situ on the unmodified membrane/pore. It is well recognized [28] that the solution phase data would be superior even to crystallographic or conductance data since the former can handle even dynamic functional states (including molecular breathing) while the crystal data would be of fixed molecules averaged out of information arising from dynamics. This is important because an effective pore radius need not be, nor is, generally static [23–25,29].

An unusual application of this technique was exemplified in the studies on mitochondria wherein the porosity of the mitochondrial inner membrane was shown to vary with respiration and ATP hydrolysis [25,30–32]. This variation was traced rigorously to the presence and induction of voids in the inner membrane by respiration and ATP hydrolysis [33]. These studies also revealed for the first time that the well known phenomenon of mitochondrial swelling is not one of water imbibition but one of colloidal swelling due to porosity induced by respiration and surface charge density [31].

In mitochondria as well as in bacteria, the problem is of a double membrane. Each of the membranes have their own permeability. Generally the inner membrane, which is a true plasma membrane would be far less permeable than the outer membrane. In the presence of a double membrane, it is therefore convenient methodologically as well as biologically that the outer membrane is more porous since the probes of porosity can be approached from the outside permitting a sequential sampling first of the outer membrane and then the inner membrane. Such a logic gave rise to insights into the nature of water in the intermembranous domain indicating the presence of osmotically sensitive water, for which other techniques were ineffective [34].

The bacteria, on the other hand present a new class of problems as yet unattended to. A series of methodological questions were addressed to resolve the question of determination of porosity of membranes. The equivalent pore is not a structurally fixed pore and its structure can only be guessed. However, it represents the best approximation of a pore, which, had it existed as a fixed entity would account for the friction experienced by any or all the various solutes as a unique radius. It is a measure of limits to permeation and not average permeation, the latter being given by crystal radii and related tools. The problems are initially defined, solutions identified and applied specifically to past and current data to resolve the problem of bacterial porosity.

3.2. Renkin's equation [35] in the determination of pore radius

The measurement of equivalent pore radius only requires two pieces of information: (i) the molecular masses of the probe molecules and (ii) the flux rates (cf. [23]). The osmotic pressure exerted by a solute relates to the reflection coefficient such that

$$1 - \sigma = A_{sf}/A_{sw} \tag{3}$$

where the reflection coefficient (σ) relates to the area available for filtration (the terms A_{sf} and A_{sw} refer to the apparent areas of filtration available for solute and water, respectively), these fractional areas in a homoporous and homogeneous membrane with idealized pore geometry can be written as

$$A = A_o\left[2(1-(r/R))^2 - (1-(r/R))^4\right] \times\left[1 - 2.104(r/R) + 2.09(r/R)^3 - 0.95(r/R)^5\right] \tag{4}$$

where A_o is the geometrical pore area in the membrane, R is the radius of the pore and $A = A_{sf}$ if 'r' refers to the radius of the solute (r_s) and $A = A_{sw}$ if 'r' refers to radius of water molecule (r_w) [25,37]. The theoretical external osmotic pressure exerted by a solute as judged from its colligative properties, requires a correction, the reflection coefficient, σ.

Thus the equivalent pore radius, R, can be determined provided the radius of solute (r_s) and radius of water (r_w)

are known. The non-linear relationship between activity and molecular mass due to reflection coefficients arises only from these parameters as in Renkin's equation and can be by-passed in computations by determining a theoretical set of $1-\sigma$ values for all non-electrolytes at all pore radii [25]. Further, any osmotically dependent activity, P, can then be simply written in the linear form as

$$P = m \cdot (1-\sigma) + c \quad (5)$$

Thus, as shown earlier [25], an equivalent pore radius for any membrane can be assessed in so far as a linear osmotic dependence could be detected for a relevant membrane-dependent process. This model requires solving iteratively for the best guess of the pore radius for given activities with solutes of different molecular mass but the same external osmolality [25]. The equivalent pore radius was estimated by comparison of experimental permeability and $1-\sigma$ obtained at different pore radius. The validity of this methodology has been extensively discussed earlier [25].

Any flux measurement yields a measure of the permeability provided some simplifying assumptions are made. These assumptions ultimately decide which is a good method to assess the pore radius since each method involves different kinds of data manipulation. The primary requirement is to assign the Renkin's equation to handle the non-linear relationship between the observed flux and molecular mass.

Briefly the procedure for the determination of any porous membrane is summarized thus:

Step 1. Preparation of a set of $1-\sigma$ values for the required range of electrolytes: Obtain the radii of the non-electrolytes (actually used in the experiments) and that of water from the geometric mean of the diameters of molecular models/computer models [23] or by using empirical relationships between molecular mass and volume [25].

Step 2. Carry out regression analysis of the stretch sensitive experimental data at each pore radius for the best fit and plot the residual sum of squares (normalized to variance, NRSS) (vide infra) as a function of pore radius to assess the best pore radius.

A program is available that carries out all these steps to obtain a plot of NRSS vs. pore radius. A theoretical investigation has been added to this by doping univariate errors to create data of required form and pore size.

Two major variations need to be considered here. The first relates to stretch sensitive activities as a proxy for flux measurements. The second relates to simulation studies for similar purposes.

3.3. Stretch-sensitive activators of membrane bound enzymes

Several membrane-dependent activities appear to be stretch sensitive, i.e., these vary with osmotic stretch and therefore are a measure of the felt osmotic pressure by the membrane. Often a linear relationship is found between such activities and osmotic pressure. Respiration is stretch activable [31,36]. The osmotic sensitivity of electron transport in mitochondria [31], chloroplast [37], plasma membrane respiration [38] as well as aerobic bacterial respiration as in *E. coli* [39], involve passage of electrons over the corresponding quinone. It was demonstrated from our laboratory that it is the voids required for quinone migration which disappear on osmotic compression of the membrane [33]. Voids are compressible by definition since molecules per se cannot be compressed and the voids form a large component of the hydrocarbon phase that characterizes biological membranes [40]. Larger voids would be more compressible than smaller voids, the ultimate result being lack of spaces for the quinones or side chains of proteins, all of which contribute to the essence of diffusion control of reactions in the membrane phase [33,41]. Thus, these considerations render a linear inhibition of activity as a legitimate expectation. The relationship is generally stated thus [30,31],

$$J = J(\max/\min) \pm \tilde{K}\,\Pi \quad (6)$$

Respiration in microbes resides in the cytoplasmic membrane and obeys the relationship:

$$J_{ox} = J_{ox}(\min/\max) \pm \tilde{K}\,\Pi \quad (7)$$

where $J_{ox}(\min/\max)$ is the minimal or maximal respiration and $\tilde{K}$ is an empirically determined constant coupling by appropriate sign, the activity, J (respiration in this case), to external osmotic pressure Π [5,25,30,31,39]. This osmotic pressure–activity relationship is linear only within bounds of the external osmotic pressure for a particle (which cannot expand or contract indefinitely). The linear limit of osmotic inhibition may be obtained as a classic case of switching regression as the break-point [5,30–33,36,37,39,42–45], where the break-point offers a material constant specific for the activity measured and the physical state of the membrane. The slope is a measure of the osmotic sensitivity of the measured variable. Measurement of any membrane-specific enzyme activity, if stretch sensitive, yields an excellent marker for that specific membrane and accurately reflects the osmotic state (contraction or expansion) of that membrane. Therefore, these measurements also serve as a measure of permeability specific to each membrane. Any point on the slope of inhibition as well as the break-point are a measure of the reflection coefficient to the external solute and specific to the membrane at which the measured activity resides [25]. Thus respiration offers cytoplasmic membrane-specific measurement in bacteria to be contrasted with the packed cell volume measurements, which relate to the outer membrane [5,39].

It is simple to obtain equivalent pore radius from such stretch sensitive measurements since Eqs. (5) and (6) readily relate

$$c = J(\max/\min) \quad \text{and} \quad m = \pm\tilde{K} \quad (8)$$

depending on the sign of $\tilde{K}$. The iterative procedure of pore radius determination yields a measure of the variations in the observed osmotic pressure across that particular membrane subjected to stretch and consequently the pore radius, provided that another outer membrane limiting the access of the solute to this membrane has a barrier cut-off less than itself.

With this background, it is now possible to state formally the models for pore radius estimation and to arrive at the relative superiority of different models. These would explore the available experimental data as well as simulated data mentioned above.

3.4. Model 1

This (our) model involves the comparison of experimentally observed solute permeability (directly measured or via PCV measurements etc.) and $1-\sigma$, by a linear relationship (see Eq. (6)). $1-\sigma$, which accounts for the non-linearity between molecular mass and permeabilities is calculated independently at varying pore radii. The permeability from this linear relationship at different pore radii is back calculated and compared for identity with the experimentally observed permeability to obtain a best estimate of the pore radius as the one with the least residual sum of squares. This latter comparison requires further use of appropriate statistical procedures specified below.

The comparison of experimentally observed permeability (Y_{exp}) and that of theoretical permeability (Y_{theor}) was done by calculating the residual sum of squares (RSS) and dividing it by a sum of squared deviations from the mean, calculated for experimentally observed permeability. This ratio is referred to as 'normalized residual sum of squares' (NRSS). The 'least-squares' estimate of the unknown R (pore radius) is obtained by minimizing this NRSS such that,

$$\mathrm{NRSS} = \frac{\sum_{i=1}^{n} \left(Y_i - f(R, r_i)\right)^2}{\sum_{i=1}^{n} \left(Y_i - \bar{Y}\right)^2} \qquad (9)$$

where n is the number of observations, Y_i is the experimental permeability with $\bar{Y}$ as a mean of that and $f(R,r_i)$ refers to Renkin's equation, which in this model relates to $1-\sigma$ and in turn to the theoretical permeability. The meaning of NRSS in terms of theoretical 'best fit' can be easily understood if we compare the NRSS with the correlation coefficient (r) [46]. As seen from the Eq. (9), the NRSS = $1-r^2$ for linear regression i.e. if the theoretical and experimental data are identical, then NRSS = 0. If the calculated RSS is greater than the sum of the squared deviations from the mean of the experimental data then NRSS > 1, indicating a unacceptably poor fit.

3.5. Model 2

The model published by Nikaido and Rosenberg [20] computes rates of diffusion theoretically based on the following version of Renkin's equation as a product of diffusion in water and the area available for filtration.

$$P = D \cdot (a/a_0)$$

where,

$$a/a_0 = [1-(r/R)]^2\left[1 - 2.104(r/R) + 2.09(r/R)^3 - 0.95(r/R)^5\right]$$

and

$$D = KT/6\Pi\eta r \qquad (10)$$

where P is the permeability, r is the solute radius and R is the radius. D is the diffusion coefficient, K is the Boltzmann constant, T is the absolute temperature, and η is the coefficient of viscosity.

These authors obtain theoretically expected permeability for varying pore radii and use them for fitting to the experimental data *apparently by a visual fit* to estimate the pore radius. This we have made more quantitative to enable one to rigorously compare the theoretical versus the experimental data by calculating NRSS as described in model 1.

The major limitation in model 2 was the lack of appropriate statistical procedures considering the small sample sizes (in some instances as small as four sugars! (cf. [20]) involved in fitting such an equation of high power functions. An alternative and even more arbitrary model used by Nikaido and co-workers was the exclusion limit in molecular mass by projecting the permeability data in a log scale [18]. In fact, logarithmic transformations cannot yield straight lines of any respectable kind for these non-linear phenomena even for scanty data! Use of nonparametric tests will help in identifying pattern in residuals after fitting a linear regression. In particular, too few runs in the residuals are indicative of inadequacy of the linear fit (non-linearity of the model). In such a situation extrapolation (projection) may give totally misleading conclusions. However, one requires a larger data set than what is generally available in these classes of experiments (i.e., $n > 15$). Similarly, Nakae and co-workers also have used the logarithmic scale for molecular mass and proposed the exclusion limit [14–16,47,48], and this has been debated in the literature [18]. Exclusion limits obtained by extrapolation therefore would be too gross to be of real analytical value.

It was well known that in the absence of a precise geometry of the path of diffusion, an exact quantitative description of the pore would not be possible [25,29,49]. It was also recognised that Renkin's equation was an adequate descriptor of the equivalent pore radii for pores [25]. Therefore it becomes necessary at this stage to check the

predictivity of each of these equations used in model 1 and 2. We also consider that the experimental data is likely to be error-prone and the distribution of these errors is strongly dependent on the kinds of transformation performed on the measured variables during pore size estimation. Thus two kinds of tests become critical in any model: firstly, how do the equations behave for theoretical data when these are doped with univariate error? Secondly, when an experimental system is calibrated using known molecular masses, how good is the prediction (really postdiction) of molecular masses from each of the equations? Obviously, theoretical data generated by one model cannot be used to evaluate the worthiness of the other and therefore we have throughout used theoretical data sets generated separately for each model. Further, the goodness of fit requires some universal test which is independent of the kind of equations used to model the process. One such is that the residual sum of squares of the experimentally derived data from the theoretical data generated after the best fits are compared. The residual sum of squares are scale dependent, they are therefore divided by the variance of the system to obtain the normalized (scale-free) residual sum of squares (NRSS) (see Eq. (9)). This could be used gainfully to compare different models, including the quality of digitization of the published data! The importance of NRSS is in that if the residuals were truly random (i.e., the data has no additional pattern other than normally distributed random errors), it can never exceed 1.0, i.e., fitted data would always have variation less than or equal to the total variance of the data. Regardless of the expression used, NRSS would always tend hyperbolically to 1.0 in the case of normal errors but never exceed 1.0 (see below). On the other hand, if the NRSS exceeds 1.0, it is certain that the model is bad (regardless of whether the data are good or bad).

3.6. Theoretical permeation data for varying pore radii using different models

Fig. 2 represents theoretical permeation data by model 1 (Fig. 2A) and model 2 (Fig. 2B). The permeability data were obtained using a straight line relationship between solute radius and permeability, Stokes–Einstein equation (Eq. (10)) and data for a pore radii of 6 Å and 15 Å. The data were analyzed using model 1 as well as 2. A plot of NRSS versus pore radius (R) was used (Fig. 2C and Fig. 2D) to locate the least-squares estimate, R. This is feasible when NRSS is a sharply convex curve. However, it is not generally realized that Renkin's equation is applicable only within the upper bounds of pore radii 12–15 Å. Fig. 2C and Fig. 2D. illustrate the NRSS profiles for 6 Å and 15 Å pore radii. One sees that at a pore radius of 15 Å, the NRSS does not again increase and remains flat. At much higher radii and when data have some error (as seen on doping with univariate Gaussian error), the data becomes even less decipherable (data omitted). All that one can do

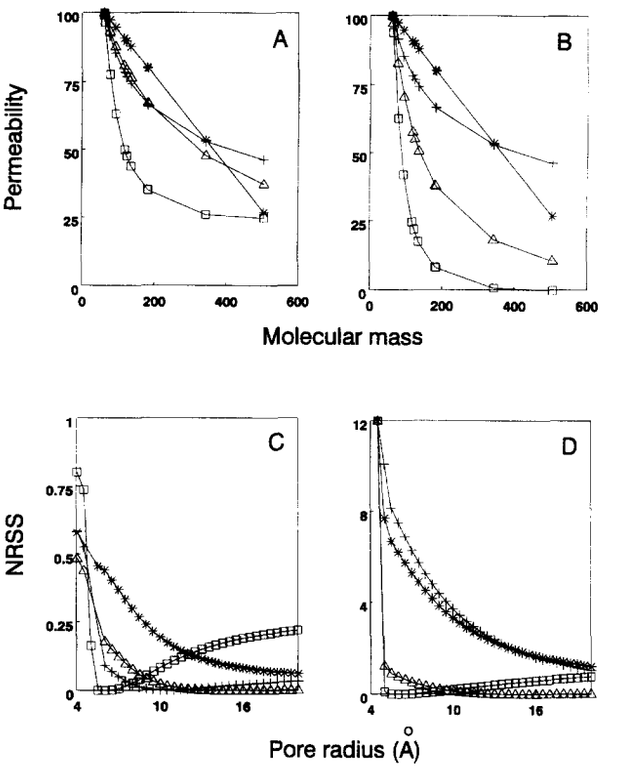

Fig. 2. Simulation studies on limits of Renkin's equation. Limits of Renkin's equation were tested by generating theoretical data of permeability for 12 non-electrolytes (see Section 2.2 and Fig. 7). The theoretical permeability (P) was calculated by using the equations of model 1 (A) and model 2 (B). The equation of model 1 is $P = m \cdot (1 - \sigma) + c$, where, $m = 100$ and $c = 10$. The permeability was calculated by assuming that these non-electrolytes are diffusing through a pore of a radius 6 Å (□), 15 Å (△). Similarly the diffusion coefficients of these non-electrolytes in water were normalized to the permeability (+) and these were also tested. A given linear relationship of $Y = m \cdot X + c$, between permeability and molecular mass was also used (*) where, $m = -1.5$ and $c = 1000$. The data was normalized to the permeability value of urea, a smallest molecular mass non-electrolyte used for this simulation. Each of these data sets were subjected to the pore analysis to guess the pore size by computing the NRSS at varying guesses of pore radii by both model 1 (C) and model 2 (D). The correct guess of pore radius would yield the lowest NRSS (= 0) as a means to identify the pore radius.

is to judge the smallest R after which significant drop in NRSS no longer occurs. A reasonable estimate of this R may be obtained by using break-point analysis [42].

The lack of a clear $NRSS_{min}$ in some data sets complicates the problem. Typically we may consider an experiment, wherein permeability data are available for the native membrane (control) and the membrane is treated with an agent, which affects the pore size. This requires that one evaluates the data in many ways. Firstly, if the permeability data of membrane treated with an agent is consistently higher (or lower) than for the control at most values of molecular masses, then the effect of the treatment can be judged to be significant using a binomial test (or any suitable non-parametric test). Secondly, one should apply an NRSS procedure and determine that the NRSS profile

changes 'self-evidently' between the control and the treated. Herein lies the importance of simulated data with and without error doping, a practice rarely used in biological literature! Lastly, one may use the break-point procedure to identify or 'test' (a very weak notion statistically speaking, since this is not true data but obtained only theoretically!). It may however be adequate to accept the null hypothesis, the equality of the R (corresponding to $NRSS_{min}$) between the treated and the untreated. It is generally advisable, due to limitations of non-linear regression methodology, to consider a large number of computed data points (in excess of 100–150 per arm) while applying the bootstrapping procedures to estimate the differences in pore radii (cf. [42] and the cross references therein) give the necessary details that one should consider before applying such procedures. It suffices to recognize that this is a difficult problem not fully resolved within the framework of the statistical theory itself.

Fig. 2 thus illustrates that: (i) Model 2 was very sensitive to the model chosen and clearly yielded NRSS > 1.0 for permeability data obtained from a straight line and the Stokes–Einstein diffusion equation. (ii) Model 1 gave consistently low NRSS values. (iii) As pore radii exceed 10 Å, the minima were not discernible by either model. Pore radii were conservatively estimated as an approximation as the lowest NRSS at the smallest pore radius. Thus model 1 exhibited less sensitivity to modelling errors, but a better profile of minimum of NRSS in a range of pore radii below free diffusion.

3.7. Influence of error doping on the pore size estimation

We next investigated the error susceptibility of the models at various data sizes, since pore size estimations in literature have used as few as four sugars [20]. The objective was to dope the error on the theoretically generated permeability data set and estimate the pore size by both models 1 and 2. The error was univariate and Gaussian, and the procedure was as follows.

Initially theoretical permeation data were generated on appropriate equations as described in models 1 and 2. These theoretical data were doped with error on Y (i.e., permeability) such that the error was univariate Gaussian, thus. Firstly, the % error was defined by normalizing the variance (σ^2) in the theoretical permeability data to 100% and σ_1^2 was calculated as

$$\sigma_1^2 = \frac{\sigma^2 \cdot \%\,\text{Error}}{100} \tag{11}$$

The data (Y_i) was sequentially doped as follows,

$$Y_i(\text{Doped}) = Y_i(\text{Theoretical}) + E_{(i)}$$

where $E_{(i)}$ is error term and,

$$E_{(i)} = Z \cdot \sigma_1 \tag{12}$$

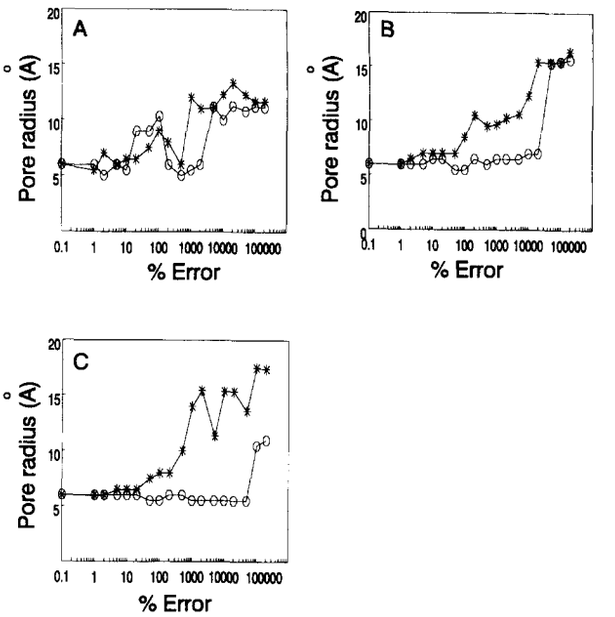

Fig. 3. Influence of error doping and number of data points on the guess of the pore size. The theoretical permeability data for 6 Å pore radius were generated using the equation of model 1 and model 2. Different non-electrolytes with non-overlapping molecular masses were used to check the influence of number of data points. The equation used for model 1 is $P = m \cdot (1 - \sigma) + c$, where, $m = 100$ and $c = 10$. The data were doped with different levels of univariate Gaussian errors and pore radius from such doped data sets was estimated by model 1 and 2 (see text). The % error is plotted against the pore radius in angstrom. Pore estimation by model 1 (○), model 2 (∗). (A) Plot generated using the data set of four non-electrolytes (cf. [20]). (B) Plot generated using the data set of 12 non-electrolytes (cf. Fig. 7). (C) Plot generated using the data set of 19 non-electrolytes.

where Z is the Box–Muller transformation [50] to get two standard normal deviates for given uniform variates U_1 and U_2. The values of U_1 and U_2 were generated by using a random number generator.

The next step is to generate a number of data sets at different % levels of error and determine NRSS. Fig. 3 shows pore size as a function of magnitude of error for 4 (Fig. 3A, as in Ref. [20]), 12 (Fig. 3B, as in this manuscript) and 19 (Fig. 3C, which would represent a major available selection of polyols commercially available in this molecular weight range) polyols. (i) Clearly, susceptibility to error depends both on magnitude of the error and on paucity of data regardless of the model; and (ii) the error susceptibility of model 1 was less than that of model 2 (though the data for each model was generated only by the corresponding equations). Comparable simulations in enzyme kinetics readily show that Cornish–Bowden plots [51] and Eadie–Hofstee plots [52] reign supreme in kinetic data evaluations having very low error susceptibility while Lineweaver–Burk plots [51] show extraordinary error susceptibility, correctly placing the relevant emphasis by the practitioners.

3.8. Calibration of the models against known molecular masses

The choice of the model for pore size determination really depends on which model predicts the molecular properties (e.g., size) better. There can be no dispute in choosing the one with the lowest NRSS among several models. The molecular masses of electrolytes and non-electrolytes were computed as a test for model 1 earlier [25] and again with model 2 of Nikaido [20] incorporating the estimates based on lowest NRSS values. Table 1 shows that while both are generally comparable, model 1 is better with regard to lower NRSS values. It may also be noted that the nature of measurement (e.g., solute flux vs. volume flux) does matter in better prediction of the molecular masses.

3.9. Effects of SDS and CTAB on turbidity changes in E. coli and Pseudomonas

Bacteria would show turbidity changes depending on three parameters: (1) permeable external solutes lead to swelling and decrease in turbidity; (2) respiration causes swelling in even isotonic solutions; addition of a stock solution of bacteria, which would be highly anaerobic and acidic (if not heavily buffered) to media would not be mere dilution but a drastic change in the environment of the bacterium, a fact well known in mitochondria [31]; (3) sugars like glucose stimulate respiration which in turn stimulates turbidity, which may relate to induction of voids in the membrane similar to mitochondrial respiration [25,33,41]. Use of sugars without monitoring respiration (cf. [21]) could thus be very misleading.

Volume changes of the bacteria can be monitored by light scatter/absorbance methodology. The optical density varies inversely with the volume of the particle and importantly, the size of bacteria permits the application of Jobst approximation [53]. This methodology was used for monitoring the permeability of an external solute through an outer membrane in intact bacterial cells. The major advantages of this procedure are as follows: (i) rate of turbidity vis-à-vis volume changes are related to the permeability of the solutes, (ii) rate of turbidity changes of the bacterial cells are dependent on the external osmolality and therefore it is possible to apply Boyle– van't Hoff relationship [45,53], (iii) it is a simple and convenient experimental procedure to handle. Fig. 4 shows the plot of specific activity (i.e., −dOD per min per mg of total bacterial protein) of turbidity changes versus detergent concentration in nearly isotonic sucrose media (300 mosmol/kg).

The rate of turbidity changes monitored in sucrose media shows changes with addition of detergents SDS and CTAB in *E. coli* (Fig. 4A) and *Pseudomonas* (Fig. 4B). If the external solute is permeable, one would observe a decrease in optical density as a function of time and therefore the specific activity would exhibit a negative sign. It is clear from Fig. 4 that, in *E. coli* and *Pseudomonas*, both detergents induce a greater decrease in optical density than the cells without detergent treatment (i.e., zero concentration). Particularly, CTAB appears to be more potent in this aspect as judged by the concentration used and the magnitude of the turbidity changes observed. It should be noted here, while interpreting the data, that

Table 1
Calibration of ionic radii of solutes based on prior knowledge of the pore radii using non-electrolytes (data based on Ref. [25])

Material	NRSS	Pore radius (Å)	Molecular mass (computed)				
			HCl 36.5 [a]	NaCl 58.4 [a]	KCl 74.6 [a]	$CaCl_2$ 111 [a]	Sucrose 342.3 [a]
Dialysis membrane							
Solute flux							
A	3.20	–	51.19	–	65.86	76.93	463.61
B	0.03	9.17	24.38	–	53.43	89.33	415.70
C	0.05	9.74	38.26	–	58.00	83.19	643.99
Volume flux							
A	1.60	–	42.40	215.90	146.92	255.10	272.01
B	0.04	8.26	38.09	231.59	266.75	276.70	342.54
C	0.15	11.79	39.24	179.23	199.92	205.31	235.94
Sephadex G-15							
A	0.005	–	37.13	80.78	–	–	356.85
B	0.003	11.25	27.06	95.70	–	–	338.15
C	1.70	21.84	20.16	33.79	–	–	62.62

(A) The molecular masses were obtained by fitting the flux rates of non-electrolytes to their molecular masses by a power function, $y = ax^b$. The molecular masses of electrolytes were obtained by an interpolation of the experimentally derived fluxes. (B) The pore radii were determined as per model 1 in the text. (C) The pore radii were determined as per model 2 in the text. The values of normalized residual sum of squares (NRSS) are corresponding to the optimal pore radius obtained in (B) and (C). The experimentally observed electrolyte fluxes were used to predict the molecular mass in (B) and (C) from their corresponding equations.

[a] These value are the actual molecular masses.

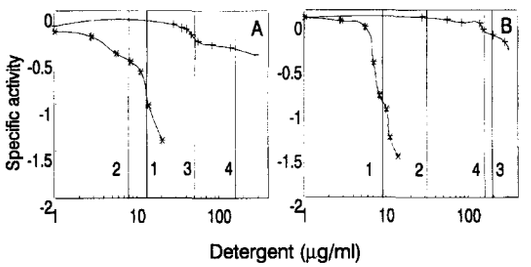

Fig. 4. Effect of SDS and CTAB on the turbidity changes of *E. coli* and *Pseudomonas aeruginosa* in sucrose media. Turbidity changes were monitored in sucrose medium (300 mosmol/kg) as described in Section 2.2. SDS (+) and CTAB (∗) concentrations are plotted against the specific activity expressed as dOD per min per mg of protein. The minus sign of the specific activity indicates the penetration of the external solute sucrose. (A) *E. coli* K12. (B) *Pseudomonas aeruginosa* NCIB 8650. The lines indicate the concentrations of the detergent used for antibiotic potentiation and the 50% effective concentrations used for experiments as in Fig. 5. Antibiotic potentiating concentrations of SDS (4) and CTAB (2), 50% effective concentrations for turbidity change of SDS (3) and CTAB (1).

volume changes in nearly isotonic medium (300 mosmol/kg) are bound to the osmotic fluxes of the solutes.

The effect of SDS and CTAB on turbidity changes in the media of different non-electrolytes of different molecular masses was investigated next, as an independent measurement of permeability. Fig. 5 shows, in *E. coli* and *Pseudomonas* the turbidity changes strictly depend on the molecular mass of the solute. Addition of SDS and CTAB resulted in enhanced permeability of the solutes of a size range 100–200 daltons and a clear potentiation of the permeability was observed, only in the case of *Pseudomonas* with SDS. These data of *Pseudomonas* when fitted to Renkin's equation yields pore radius 8.8 Å for control and 9.70 Å for SDS-treated cells. These experiments again established that addition of SDS dilates the equivalent pore in *Pseudomonas*. Importantly, the strict molecular mass dependence of turbidity changes indicate that these changes are also due to permeability changes. A major assumption in these experiments is that neither the non-electrolyte nor SDS affect the cytoplasmic membrane directly or indirectly and that the permeation experiments are devoid of the influence of the cytoplasmic membrane.

3.10. Effect of external osmolytes on bacterial respiration

Respiration would be a marker specific for the bacterial cytoplasmic membrane. Respiration, in a variety of organisms and organelles, was shown to exhibit the relationship to external osmotic pressure as in Eq. (7) [5,36,39]. Since permeation of a solute would affect the observed osmotic pressure, a correction would be required for the departure from the ideal in terms of their reflection coefficients (Eq. (3))

$$J_{ox} = J_{ox}(\min/\max) \pm \tilde{K}(1-\sigma)\,\Pi_{ext} \qquad (13)$$

Based on an osmotic titration of respiration of *Pseudomonas* in sucrose media to determine the effective range of external osmolality in which the $\tilde{K}$ can be used for a non-electrolyte (Fig. 6A), a profile of respiration at a specific external osmotic pressure was determined using non-electrolytes (cf. Fig. 6). Data in Fig. 6B shows the molecular mass dependence of respiration with an equivalent pore radius for the inner membrane, which was approx. 5.3 Å and it did not change on addition of SDS (data not given). Thus the influence of the molecular mass on the cytoplasmic membrane was clearly distinct from that on the outer membrane with regard to the effect of SDS. It

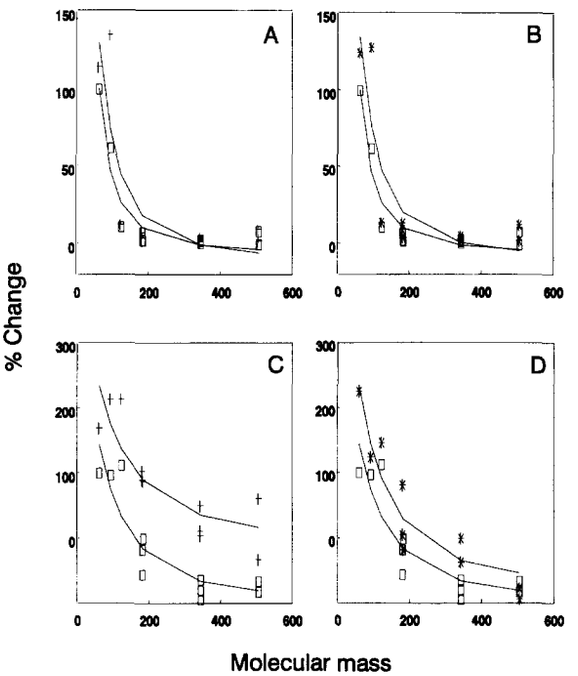

Fig. 5. Effect of SDS and CTAB on the turbidity changes of *Pseudomonas aeruginosa* and *E. coli* in different non-electrolyte media of different molecular mass. Turbidity changes of *E. coli* and *Pseudomonas aeruginosa*, NCIB 8650 were monitored in different non-electrolyte media in the presence and absence of detergents. The osmolality of the medium was adjusted to 300 mosmol/kg and specific activity of turbidity change was measured (for details see Section 2.2). The specific activities were normalized against activity obtained in control cells in the medium containing urea. *E. coli* (A,B), *Pseudomonas* (C,D). Control cells, without addition of detergents (□), SDS-treated cells (+) and CTAB-treated cells (∗). The concentration of detergents used are: for *E. coli*: (i) SDS, 50 μg/ml, (ii) CTAB, 13 μg/ml; for *Pseudomonas*: (i) SDS, 193 μg/ml, (ii) CTAB, 9 μg/ml. These concentrations were determined from Fig. 4, and they are the 50% effective concentrations for turbidity changes in sucrose medium. The curved line represents the best-fit line corresponding to the estimated pore radius. The pore radius obtained: for *E. coli*: (i) control, 5.5 Å, (ii) SDS, 6.8 Å, (iii) CTAB, 6.9 Å; for *Pseudomonas*: (i) control, 8.8 Å, (ii) SDS, 9.7 Å, (iii) CTAB, 8.8 Å. In *Pseudomonas* the larger pore radius obtained after SDS addition (C) is significantly different from the control at $P < 0.05$ by all the criteria listed in the text. The non-electrolytes and their anhydrous molecular masses are urea (60.06), glycerol (92.09), erythritol (122.12), glucose (180.16), galactose (180.16), mannitol (182.17), lactose (342.3), sucrose (342.3), trehalose (342.31), melezitose (504.44) and raffinose (504.46).

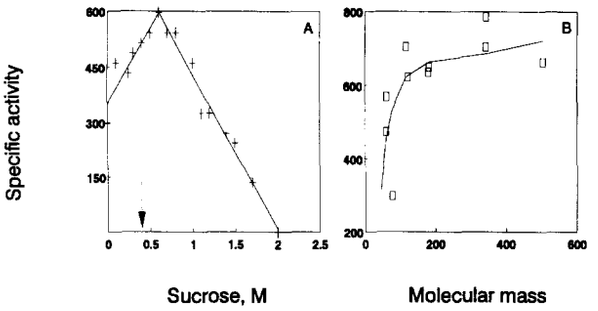

Fig. 6. (A) Osmometry of respiration of *Pseudomonas aeruginosa* (NCIB 8650) in sucrose media. Rate of O_2 consumption was monitored polarographically and expressed as nanoatoms of oxygen consumed per min per mg of protein. Respiration was monitored at different tonicities of sucrose-containing buffer A. Break-point analysis as the intercept of two regression lines was carried out as described earlier [42]. Break-point of inhibition of respiration corresponds to 0.6 M sucrose. The arrow indicates the equivalent concentrations of non-electrolytes chosen for the experiment in Fig. 6B in the osmotic domain wherein $\tilde{K}$ is positive. In this case this corresponds to the 0.4 M sucrose. (B) Respiration vs. molecular mass of non-electrolytes. The rate of respiration was measured as described in (A). The respiration was monitored in different polyols of different molecular weight. The non-electrolytes were dissolved in buffer A and their osmolality was adjusted to 530 mosmol/kg, which corresponds to the 0.4 M sucrose. Evaluation of the pore radius corresponds to 5.3 Å. The curved line represents the best-fit line at this pore size. The non-electrolytes and their molecular masses are urea (60.06), ethylene glycol (62.07), thiourea (76.12), diethyl urea (116.16), erythritol (122.12), fructose (180.16), mannitol (182.17), sucrose (342.30), trehalose (342.31) and raffinose (504.46).

should be noted that the rates of respiration measured in this study were due to endogenous substrates only. The non-electrolytes used were ineffective in stimulating the basal, endogenous respiration and therefore these measurements were devoid of interference due to additional interactions owing to induced respiration [31]. Under these conditions the observed changes in activities would be strictly due to the osmotic relationship (see Section 2.2).

3.11. Effect of SDS on the packed cell volume of Pseudomonas

Fig. 7A and Fig. 7B show the packed cell volumes of *Pseudomonas* in the absence and presence of SDS as measured by blue dextran inaccessible space. As the hypertonic non-electrolyte/polyol permeates across the cell membrane, the measured cytocrit (PCV) would be restored to the isotonic value, which represents an excellent measure of penetration of the non-electrolytes/polyol across the cell membrane. In three independent experiments in our own laboratory, the cytocrit measurements when fitted to Renkin's equation [25,35] showed an increase in the equivalent pore radius from 7–9 Å to 10–12 Å on addition of SDS (data omitted, cf. Fig. 7C).

These experiments clearly show that addition of SDS resulted in a dilation of the outer membrane matrix, and it was indeed reflected in the sieving properties of the outer membrane as seen in Figs. 5 and 7. Conceivably, the mechanism of such a relaxation could be arising from an interaction between the anionic detergent and the outer membrane resulting in some intra-molecular charge repulsion and pore dilation. We were able to assess the enhancement in (equivalent) pore radius of the outer membrane using non-electrolytes of graded molecular mass. It has been the practice in the past to assess the variable porosity using the partitioning of non-electrolytes/polyols across the outer membrane [14,15,25,47]. However, a major limitation of such studies was in eliminating the interference due to the cytoplasmic membrane effects. We therefore have used a combined strategy of turbidity and packed cell volume measurements with different non-electrolytes/polyols to determine the enhanced porosity due to the presence of SDS, while using the technique of osmometry of respiration to exclude the effect of these agents and non-electrolytes/polyols on the cytoplasmic membrane per se (vide infra).

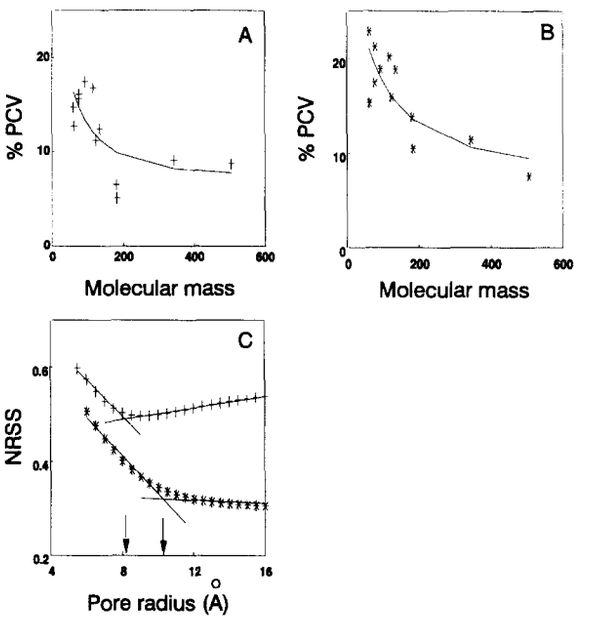

Fig. 7. Effect of SDS on packed cell volume in *Pseudomonas aeruginosa* (NCIB 8650) in the presence of various polyols of different molecular mass. Packed cell volume (PCV) measurements were carried out in triplicate as described in Section 2.2. The data are representative of three independent experiments. Each PCV value is the mean of a triplicate determination which agreed within 5%. PCV measurements in control cells (A) and cells in the presence of SDS (400 μg/ml) (B). Estimation of pore radius from data in (A) and (B), was carried out as per model 1, described in text. For detailed computational methodology see Refs. [25] and [42]. The respective curved lines in (A) and (B) represent the best-fit lines corresponding to pore radii of 8.1 Å and 10.2 Å (indicated by arrows in (C)), which differ from each other at $P < 0.05$. In three independent experiments the pore radius obtained for control cells are 9.1 Å, 7.8 Å, 9.7 Å and SDS-treated cells are 12.7 Å, 10.6 Å, 10.3 Å, significantly different from each other at $P < 0.05$. The non-electrolytes and their molecular masses are urea (60.06), ethylene glycol (62.07), propylene glycol (76.09), thiourea (76.12), glycerol (92.09), diethyl urea (116.16), erythritol (122.12), 2-deoxyribose (134.13), fructose (180.16), mannitol (182.17), sucrose (342.30) and raffinose (504.46).

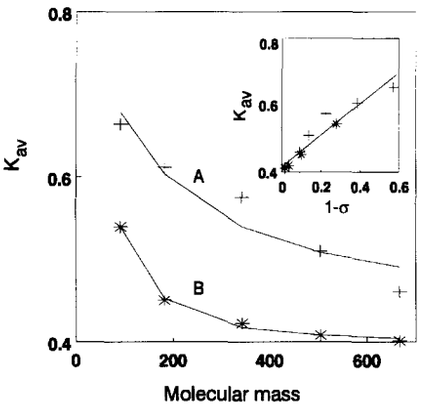

Fig. 8. Effect of ionic strength on the equivalent pore radius of DEAE-Sephadex. Solutes of different molecular mass were eluted on the column equilibrated with distilled water (A, +) and 1 M NaCl (B, *). The K_{av} value is plotted against the molecular mass of the solutes. The solid line represents the theoretical line obtained for pore radius 12.8 Å (A) and 7.5 Å (B). K_{av} values of both A and B were further used to calculate the $1-\sigma$ at their corresponding optimal pore radius. The inset shows the linear relationship between experimentally observed K_{av} values and $1-\sigma$. Regression coefficient = 0.9692, $P < 0.001$. The non-electrolytes and their molecular masses are glycerol (92.09), mannitol (182.17), sucrose (342.30), raffinose (504.46) and stachyose (666.6).

3.12. Enhanced permeation due to charge repulsion-example of DEAE-Sephadex chromatography

It remained to be shown that charge repulsion could indeed enhance porosity that can be detected by the same techniques used thus far. An elegant example would be chromatography with DEAE-Sephadex pre-equilibrated with media of different ionic strengths. Fig. 8 shows that low ionic strength not only enhanced the K_{av} for polyols but also enhanced the equivalent pore radius. As K_{av} is a normalized measurement, it was not surprising that the m and c (Eq. (5)) were indistinguishable and represented a common line when corrected for different optimal pore radii (Fig. 8, inset). Thus the seven equivalent pore measurements are not only realistic but well suited to a physical interpretation. Most importantly, these results verify the physical theory inherent to ionic strength/charge effects in a defined system as an experimental and analytical parallel to the studies on bacteria.

4. Discussion

The criteria for the choice of a model become more stringent as the model gets more sophisticated. Assessment of pore radius reflects a complex evaluation of the experimental data at a level commensurate with the underlying theory. These are delineated here for the first time.

4.1. Criteria for choosing between alternative models

Compared to our own published model [25] which consistently yields 20–30% lower estimate of the pore size, the now revised model 1 yields nearly the correct value for pore sizes below 10–15 Å, as does model 2. When we compute the diffusion data (in water) for these molecules based on Stokes–Einstein equation and attempt to solve for the pore radius as in model 1, we obtain a value of ≈ 13 Å, which would be the limiting case for detection of aqueous pores by these techniques!

Our revaluation of the data on *Pseudomonas* surprisingly indicated that the data published by Nikaido's group and Nakae's group were neither mutually inconsistent nor even of poor quality! In fact, as shown in Table 2, their data often give excellent fits when properly treated statistically. It should be noted that the data reanalyzed in Table 2 represent all the data that we could obtain from published studies. Table 2 yields the following conclusions: (i) The model of Nikaido (i.e., model 2) yields a larger pore size than our model (model 1) in general. (ii) Model 1 is consistently superior to model 2 in terms of normalized residual sum of squares, robustness in the face of errors and consistency even in the face of diverse assays. (iii) In general, swelling experiments perform well, while sugar retention, pellet weight or penetration assay perform poorly particularly with model 2. (iv) The impression is distinct that whenever NRSS is very low and data good, the equivalent pore radii estimates in different experiments/laboratories are very consistent, be it a liposomal assay or be it based on intact cells. (v) The coherence between liposomal assays and turbidity assays in intact cells is striking. *E. coli* appears to have a lower pore size than *Pseudomonas* by either model. Their exact sizes would be a matter of debate unless all authors use the same assay and, equally importantly, the same analytical/statistical procedures. The overall conclusion does favour the model we have used in this paper. It is also important to note that induced changes in pore size were more readily assessed by model 1 than model 2.

4.2. Estimation of errors in the data

Fig. 9A illustrates an example where the theoretical permeability data was generated for a set of non-electrolytes by assuming that they are permeating through a pore of 6 Å radius. Such data was doped with different % univariate Gaussian errors and the NRSS obtained at the 6 Å pore radius was calculated by both models 1 and 2. When NRSS was plotted as a function of error doped it behaved in a hyperbolic manner tending to 1.0. Thus, within the constraints of the relationships, the NRSS value of 1.0 cannot be exceeded for a given relationship and if the NRSS exceeded 1.0 for a given set of data it would necessarily mean that the given relationship would be inadequate to explain the data. Model 1 consistently gave a lower NRSS value than model 2, suggesting that model 1 is less susceptible to errors.

In published literature several methods have been used to monitor permeability across bacterial membranes (cf.

Table 2). These measurements can be broadly classified as: (i) Rate measurements of volume changes of intact bacteria or of porin-incorporated liposomes, e.g., liposome swelling, light scatter/turbidity measurements. (ii) Measurements where rate is not directly measured but inferred by measuring either the pellet weight, PCV and extent of penetration of solutes. It was possible from the plot in Fig. 9A to assess the % error based on the NRSS value in the experimental data listed in Table 2. The objective was to analyse the % error in the experimental data obtained by different measurements of permeability. Fig. 9 (B and C) shows a scatter plot of % error associated with different measurements. The features of the scatter plot are: (i) Different measurements have varying levels of errors associated with them. (ii) Our own measurements of PCV showed errors as large as the liposome swelling measurement (Fig. 9B). (iii) Penetration assay and pellet weight measurements showed large error, when analysed by model 2 (Fig. 9C). (iv) Growth parameters consistently showed low errors for both models, although it cannot be a direct measurement of permeability.

In order to appreciate what constitutes a good measurement in 'porosity' of a membrane, certain minimal criteria need to be defined biologically as well. The statistical and analytical arguments have already been summarized.

(1) Permeability relates to frictional coefficients that define the path of the probe molecule. Renkin's equation is an approximate and yet adequate tool to handle this in the

Table 2
Comparison of the estimation of the pore radius by different models

Material	Measurement	Ref./Fig.	Pore radius (Å)		NRSS
			Model 1	Model 2	
Pseudomonas aeruginosa					
(1) H103 outer membrane	Liposome swelling	[18]	11.8	14.3	A < B [c]
(2) Protein F, purified in non-ionic detergent	Liposome swelling	[18]	14.7	13.8	A < B
(3) Protein E2	Liposome swelling	[18]	6.0	6.0	A ≤ B
(4) PA01 porin purified in cholate	Liposome swelling	[19]	9.6	10.3	A < B
(5) *P. aeruginosa* porin + egg phosphatidylcholine	Liposome swelling	[19]	5.0	6.0	A < B
(6) PA01 porin vesicles	Sugar retention	[17]	36.5	42.4	A < B
(7) Protein C, D, E	Liposome swelling	[16]	5.0	5.0	A < B
(8) Proteins of PA01 outer membrane. Liposomes containing Dextran T-70, stachyose	Liposome swelling	[48]	5.5	5.5	A < B
(9) Outer membrane proteins of F-sufficient strain PA01 and F-deficient strains KG-1077, 1078, 1079, 1081	Liposome swelling	[48,8]	5.5	5.5	A < B
(10) Intact cells under the condition of 600 mosmol/kg NaCl	Penetration assay	[15]	9.3	18.8 [b]	A < B
(11) Intact cells	Pellet weight	[15]	6.0	16.8 [b]	A < B
(12) Intact cells-H103 strain	Light scattering	[21]	13.3	14.0	A < B
(13) Intact cells-Opr F deficient mutant H636	Light scattering	[21]	11.8	11.5	A < B
(14) Intact cells (Control)	PCV measurement	Fig. 7	8.1	11.2 [b]	A < B
(15) Intact cells + SDS	PCV measurement	Fig. 7	10.2 [a]	12.8 [a,b]	A < B
(16) Intact cells (Control)	Turbidity measurement	Fig. 5	8.8	7.8	A < B
(17) Intact cells + SDS	Turbidity measurement	Fig. 5	9.7 [a]	11.7 [a]	A < B
(18) Intact cells + CTAB	Turbidity measurement	Fig. 5	8.8	8.8 [a]	A < B
Escherichia coli					
(19) OMP F porin	Liposome swelling	[18]	5.0	5.0	A < B
(20) *E. coli* porin	Liposome swelling	[20]	5.1	6.0	A < B
(21) Intact cells	Growth parameters	[20]	5.0	5.0	A < B
(22) Outer membrane of *E. coli* B	Liposome swelling	[48]	6.5	7.7	A < B
(23) Intact cells	Pellet weight	[15]	15.3	19.4 [b]	A < B
(24) Intact cells	Penetration assay	[15]	15.4	22.4 [b]	A < B
(25) Intact cells (Control)	Turbidity measurement	Fig. 5	5.5	5.5	A < B
(26) Intact cells + SDS	Turbidity measurement	Fig. 5	6.8 [a]	8.2 [a]	A < B
(27) Intact cells + CTAB	Turbidity measurement	Fig. 5	6.9 [a]	7.8 [a]	A < B
Mycobacterium chelonae					
(28) Purified 59 kDa protein	Liposome swelling	[1]	9.9	10.6	A < B

Pore radius was estimated by model 1 (A) and model 2 (B) as in the text.
[a] Pore radius is statistically different from their control at $P < 0.05$. [b] NRSS > 1. [c] A < B indicates that model 1 is superior to model 2, otherwise both are comparable.

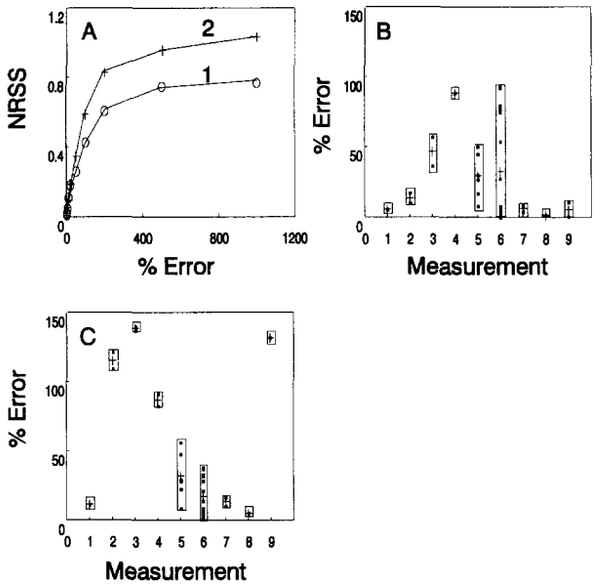

Fig. 9. Assessment of errors in the experimental data. (A) The theoretical permeability data for 6 Å pore radius were generated using the equations of model 1 and 2. The 6 Å pore radius was chosen as a representative. The equation used for model 1 is $P = m \cdot (1 - \sigma) + c$, where, $m = 100$ and $c = 10$. The data were doped with different % levels of univariate Gaussian errors (see text). The NRSS was computed for such data at varying guesses of pore radii given the permeability data constructed as above. A hyperbolic curve shows the NRSS obtained by model 1 (curve 1) and model 2 (curve 2). Similar hyperbolic curves were obtained for different pore radii (data omitted). The hyperbolic curves 1 and 2 were fitted to the linear equation $Y = mX + c$ in a reciprocal plot. The equation for curve 1 is $Y = 92.71 \cdot X + 1.88$, regression coefficient = 0.9937. Curve 2, $Y = 123.42 \cdot X + (-0.8553)$, regression coefficient = 0.9966. The error in the data listed in Table 2 was estimated from the NRSS obtained at the best pore radius by model 1 (B) and model 2 (C). Numbers denote the different types of measurements and these are as follows: (1) sugar retention assay, (2) penetration assay, (3) pellet weight measurement, (4) packed cell volume measurement, (5) turbidity measurement, (6) liposome swelling method, (7) light scatter measurement, (8) growth parameters, (9) gel filtration (cf. Fig. 8). The data points in the figures represent the error in the experimental data listed in Table 2. The average of the error is indicated by the plus symbol. The box represents the total variance in the data.

form of $1 - \sigma$. The implicit assumptions are clear: the pore is merely an equivalent pore, which confers a 'relationship' between permeability of the solute (in terms of frictional drag experienced by the solute) and its molecular mass. The pore is not to be interpreted in the literal sense, but would be a path of defined geometric and fluid dynamic approximation (such as a laminar flow of the solvent) and can be considered only in statistical terms.

(2) Since the non-linear dependence of molecular mass largely resides in frictional coefficients, the observed fluxes (P) should relate to $1 - \sigma$ in terms of two empirical factors m and c, which confer appropriate scaling and dimensionality for the sieving process, leading to a single expression (Eq. (5)),

$$P = m \cdot (1 - \sigma) + c$$

In the debate that exists on the pore sizes in *Pseudomonas* vis-à-vis *E. coli* [14–19,47,48], the high molecular radius of *Pseudomonas* pores with lower flux [18] was never adequately explained. Analysis as in Eq. (5) would be linear only at the correct pore radius, thereby accounting fully for the frictional coefficients for the solute through the pore. Net flux depends on 'm' as well as 'c' based on different mechanisms. If the amount of protein (porin) is the same, variable 'P' must imply variation in open/closed channels. Thus, our analysis forces the search for gating of *Pseudomonas* pores (as also may be the case in *Mycobacteria*! [1]), if one must reconcile the physical theory with the experimentally observed fluxes. Unfortunately, discussion in literature has distinctly blurred the relative weightage to each of these terms, P, $(1 - \sigma)$, m and c. *If a particular antibiotic / solute has higher permeability than seen with Eq. (5), then it would indicate a specific uptake mechanism, while significantly lower net uptake would mean active efflux as one may see in case of multiple drug resistance* [4]. This model is illustrated graphically in Fig. 1 and thus these measurements uniquely help in cellular kinetics associated with antibiotic action. The frictional coefficients that define $(1 - \sigma)$ may not be defined fully unless the geometry of the pores is known. Yet, actual studies revealed that corrections required would be only marginal [29]. However, the description of a pore is statistical, while the 'statistic' regarding its distribution (intrinsic to a single pore as well as inter-pore heterogeneity) remains largely unknown. Thus much of the debate in literature should be viewed with circumspection.

(3) This analysis further limits the conclusions that one can draw reliably from molecular mass dependence and the flux measurement made. For instance, any variable (e.g., respiration) that is osmotically dependent, could substitute for P with corresponding changes in the dimensionality in terms of m and c. However, if the observed fluxes are far removed from osmotic fluxes (e.g., growth [20]), it would not be prudent to argue which is a better measurement, growth or packed cell volume. Even for a solute flux versus volume flux across dialysis membranes, we observed that solute flux was a better measurement for $1 - \sigma$ and equivalent pore estimations than volume flux (Table 1).

These results have brought to focus a distinct possibility that interaction of charged species would be involved in an explanation for the action of SDS on *Pseudomonas*. For the specific purpose of obtaining drug combinations, the need for an a priori knowledge of the mechanism is not really required in so far as the compounds are acceptable drugs for a given route of administration.

These studies have immediate importance for two reasons. Firstly, despite possible innumerable interactions, the modulation of molecular sieving involved in potentiation by SDS could be identified with the outer membrane unequivocally. A better resolution of the mechanism at the molecular level using liposomes reconstituted with specific

porins would also need to be pursued with the caveat that such reconstituted structures may or may not exactly duplicate the behaviour of the native structures due to the presence of the detergent. Indeed, much of the current experimental strategy was specifically designed to overcome this limitation by examining the behaviour of organisms per se rather than reconstituted structures. Various bacterial porins have been described to exhibit various diameters, strikingly of a comparable range as reported here: maltoporin of 5–6 Å [54], PhoE and OmpF, 11×7 Å at the constriction in the open state [28], *R. capsulatus* porin at $\approx 9 \times 7$ Å [55]. The studies revealed that the constriction zone could be enhanced in diameter by site directed mutagenesis of the arginine residues at this zone and that the diameters so obtained are strongly influenced by the ionic environment and possibly the conformational states of the channel for which crystallographic data alone is highly inadequate. Thus while the porin structures show stability in the face of detergents in the sense of structural integrity, the available information is highly suggestive of modulation of porin diameters by ionic strength/ionic detergents, the latter mediating the most potent interfacial changes in the ionic strength due their interfacial preference between the protein polymer and the aqueous medium. Detailed titrations of the mitochondrial, thylakoid and erythrocyte membranes with ionic detergents were consistent with their charge screening potential of a simple Langmuir type [56] except that the affinity for the interface for the monovalent detergent species was as good as the trivalent ions, in our experience [31,32,37,57–59]. The current studies reinforce the often expressed faith [28] in the superiority of the solution phase permeability measurements in the determination of pore radius, with the added information of superior handling of errors given the right analytical methodology of a finesse and checks for internal consistency hitherto not available. Currently studies are under way to examine means of potentiation of antibiotics by adjuvants in vitro as well as in vivo and to identify drug combinations, particularly with the generics to combat infections.

Acknowledgements

The authors are grateful to Dr. S.A. Paranjpe and Dr. A.P. Gore for helpful discussions and advise on statistical treatments.

References

[1] Trias, J., Jarlier, V. and Benz, R. (1992) Science 258, 1479–1481.
[2] Nikaido, H. (1989) Antimicrob. Agents Chemother. 33, 1831–1836.
[3] Vaara, M. (1992) Microbiol. Rev. 56, 395–411.
[4] Hayes, J.D. and Wolf, C.R. (1990) Biochem. J. 272, 281–295.
[5] Sitaramam, V. and Rao, N.M. (1986) Indian J. Exp. Biol. 24, 615–623.
[6] Brawn, M.R.W. (1975) in Resistance of *Pseudomonas aeruginosa* (Brawn, M.R.W., ed.), pp. 71–107, John Wiley and Sons, London.
[7] Hancock, R.E.W. (1986) J. Antimicrob. Chemother. 18, 653–659.
[8] Gotoh, N., Wakebe, H., Yoshihara, E., Nakae, T. and Nishino, T. (1989) J. Bacteriol. 171, 983–990.
[9] Nikaido, H. and Vaara, M. (1985) Microbiol. Rev. 49, 1–32.
[10] Quinn, J.P. (1992) in *Pseudomonas*, Molecular biology and biotechnology (Galli, E., Silver, S. and Witholt, B., eds.), pp. 154–160, American Society for Microbiology, Washington, D.C.
[11] Satake, S., Yoshihara, E. and Nakae, T. (1990) Antimicrob. Agents Chemother. 34, 685–690.
[12] Trias, J. and Nikaido, H. (1990) in *Pseudomonas*, Pathogenesis, and evolving biotechnology (Silver, S., Chakrabarty, A.M., Iglewski, B. and Kaplan, S., eds.), pp. 319–327, American Society for Microbiology, Washington, D.C.
[13] Yoshimura, F. and Nikaido, H. (1982) J. Bacteriol. 152, 636–642.
[14] Yoneyama, H., Akatsuka, A. and Nakae, T. (1986) Biochem. Biophys. Res. Commun. 134, 106–112.
[15] Yoneyama, H. and Nakae, T. (1986) Eur. J. Biochem. 157, 33–38.
[16] Yoshihara, E. and Nakae, T. (1989) J. Biol. Chem. 264, 6297–6301.
[17] Hancock, R.E.W., Decad, G.M. and Nikaido, H. (1979) Biochim. Biophys. Acta 554, 323–331.
[18] Nikaido, H., Nikaido, K. and Harayama, S. (1991) J. Biol. Chem. 266, 770–779.
[19] Yoshimura, F., Zalman, L.S. and Nikaido, H. (1983) J. Biol. Chem. 258, 2308–2314.
[20] Nikaido, H. and Rosenberg, E.Y. (1981) J. Gen. Physiol. 77, 121–135.
[21] Bellido, F., Martin, N.L., Siehnel, R.J. and Hancock, R.E.W. (1992) J. Bacteriol. 174, 5196–5203.
[22] Stock, J.B., Rauch, B. and Rosemen, S. (1977) J. Biol. Chem. 252, 7850–7860.
[23] Goldstein, D.A. and Solomon, A.K. (1960) J. Gen. Physiol. 44, 1–17.
[24] Lieb, W.R. and Stein, W.D. (1986) in Transport and diffusion across cell membranes, pp. 69–112, Academic Press, London.
[25] Mathai, J.C. and Sitaramam, V. (1989) Biochim. Biophys. Acta 976, 214–221.
[26] Lowry, O.H., Rosebrough, N.J., Farr, A.L. and Randall, R.J. (1951) J. Biol.Chem. 193, 265–275.
[27] Stein, W.D. (1986) Transport and diffusion across cell membranes, Academic Press, London.
[28] Cowan, S.W., Schirmer, T., Rummel, G., Steiert, M., Ghosh, R., Paupit, R.A., Jansonius, J.N. and Rosenbusch, J.P. (1992) Nature 358, 727–733.
[29] Hill, A. (1982) Proc. R. Soc. Lond. B 215, 155–174.
[30] Sambasivarao, D. and Sitaramam, V. (1983) Biochim. Biophys. Acta 722, 256–270.
[31] Sambasivarao, D. and Sitaramam, V. (1985) Biochim. Biophys. Acta 806, 195–209.
[32] Sambasivarao, D., Kramer, R., Rao, N.M. and Sitaramam, V. (1988) Biochim. Biophys. Acta 933, 200–211.
[33] Mathai, J.C., Sauna, Z.E., Oswald, J. and Sitaramam, V. (1993) J. Biol. Chem. 268, 15442–15454.
[34] Sitaramam, V. and Sambasivarao, D. (1984) Trends Biochem. Sci. 9, 222–223.
[35] Renkin, E.M. (1954) J. Gen. Physiol. 38, 225–243.
[36] Sitaramam, V. (1992) in Biomembrane Structure and Function, The State of the Art (Gaber, B.P. and Easwaran, K.R.K., eds.), pp. 123–132, Adenine Press, New York.
[37] Pan, R.-S., Sauna, Z.E., Dilley, R.A. and Sitaramam, V. (1995) Ind. J. Biochem. Biophys. 32, 1–10.
[38] Takanaka, K. and O'Brien, P.H. (1975) Arch. Biochem. Biophys. 169, 428–435.

[39] Sitaramam, V. and Rao, N.M. (1984) EBEC Rep. 3, 555–556.
[40] Bondi, A. (1964) J. Phys. Chem. 68, 441–451.
[41] Mathai, J.C. and Sitaramam, V. (1994) J. Biol. Chem. 269, 17784–17793.
[42] Shanubhogue, A., Rajarshi, M.B., Gore, A.P. and Sitaramam, V. (1992) J. Biochem. Biophys. Methods. 25, 95–112.
[43] Sitaramam, V. and Sarma, M.K.J. (1981) Proc. Natl. Acad. Sci. USA 78, 3441–3445.
[44] Sitaramam, V. and Sarma, M.K.J. (1981) J. Theor. Biol. 90, 317–336.
[45] Sitaramam, V. and Sarma, M.K.J. (1987) J. Biosci. 11, 89–105.
[46] Snedecor, G.W. and Cochran, W.G. (1968) Statistical Methods, Oxford and IBH Publishing Company, New Delhi.
[47] Ishii, J. and Nakae, T. (1988) Antimicrob. Agents Chemother. 32, 378–384.
[48] Yoshihara, E., Gotoh, N. and Nakae, T. (1988) Biochem. Biophys. Res. Commun. 156, 470–476.
[49] Tomicki, B. (1985) J. Colloid Interface Sci. 108, 484–494.
[50] Kennedy, W.J. and Gentle, J.E. (1980) in Statistical Computing (Owen, D.B., ed.), Vol. 33, pp. 133–264, Marcel Dekker, New York.
[51] Cornish-Bowden, A. and Eisenthal, R. (1974) Biochem. J. 139, 721–730.
[52] Segel, I.H. (1975) in Enzyme Kinetics: Behavior and Analysis of Rapid Equilibrium and Steady State Enzyme Systems, Wiley, New York.
[53] Koch, A.L. (1961) Biochim. Biophys. Acta 51, 429–441.
[54] Schirmer, T., Keller, T.A., Wang, Y.-F. and Rosenbusch, J.P. (1995) Science 267, 512–514.
[55] Weiss, M.S., Abele, U., Weckesser, J., Welte, W., Schiltz and Schulz, G.E. (1991) Science 254, 1627–1630.
[56] Israelachvili, J.N., Marcelja, S. and Horn, R.G. (1980) Quart. Rev. Biophys. 13, 121–200.
[57] Sitaramam, V., Sambasivarao, D. and Rao, N.M. (1988) Ind. J. Biochem. Biophys. 25, 590–600.
[58] Sambasivarao, D., Rao, N.M. and Sitaramam, V. (1986) Biochim. Biophys. Acta 857, 48–60.
[59] Sitaramam, V. and Rao, N.M. (1991) Ind. J. Biochem. Biophys. 28, 401–407.